In situ characterization of the ferroelectric transition in $BaTiO_3$ by EELS and comparison with *ab initio* methods

V. Gallegos-Orozco, R. Martínez-Sánchez, and F. Espinosa-Magaña*

Centro de Investigación en Materiales Avanzados, S.C. Miguel de Cervantes 120, Complejo Industrial Chihuahua Chihuahua 31109, Chihuahua, Mexico

(Received 19 July 2007; revised manuscript received 17 December 2007; published 23 January 2008)

Changes in the dielectric properties during the ferroelectric transition of commercial $BaTiO_3$ powders were determined *in situ*, by analyzing the low-energy-loss region of electron energy loss spectroscopy (EELS) spectra in a transmission electron microscope, at room temperature (ferroelectric phase) and 150 °C (paraelectric phase). A comparison of experimental EELS spectra and *ab initio* density-functional theory calculations (WIEN2K code) within the generalized gradient approximation (GGA) is presented. A characteristic peak around 11 eV appears in the imaginary part of the dielectric function in paraelectric phase, which is absent in ferroelectric phase. The origin of the characteristic peak is analyzed by means of energy band structure calculations.

DOI: 10.1103/PhysRevB.77.045128 PACS number(s): 77.80.Bh, 79.20.Uv, 71.20.Be, 77.22.Ch

I. INTRODUCTION

Ferroelectric materials having the chemical formula ABO_3 have attracted an increasing attention as an important class of functional materials with a variety of present and potential applications as well as a fundamental interest in the physics of their phase transitions.[1] Among these ferroelectrics materials, barium titanate $BaTiO_3$ shows a great potential for a variety of technological applications such as dynamic random access memory, thermistors, electro-optic devices, varistors, multiplayer capacitors, etc.[2–4] Barium titanate undergoes a cubic-to-tetragonal structural phase transition at the Curie temperature T_C=120 °C. The ideal structure is a perovskite, where *A* and *B* cations are arranged on a simple cubic lattice and the O ions lie on the face centers nearest the *B* cations. Thus, the *B* cations are the centers of O octahedra, while the *A* cations lie in larger 12-fold coordinated sites. This ideal structure displays a wide variety of structural instabilities in the various materials. These may involve rotations and distortions of the O octahedra as well as displacements of cations from their ideal sites. The off-center displacements of Ti ions in the high-temperature cubic phase of $BaTiO_3$ have been confirmed by Pirc and Blinc,[5] which revealed the order-disorder dynamics of Ti ions to be coexisting with displacive phase.

From a theoretical point of view, a number of first principles calculations have been made for $BaTiO_3$ by several methods. Khenata *et al.*[6] have used local density approximation (LDA) functionals to fit the calculated pressure coefficients of energy gaps and refractive indices. Wang *et al.*[7] assert that the ferroelectricity will disappear in $BaTiO_3$ if the cell volume is decreased down to certain value. Junquera *et al.*[8] have studied structural and electronic properties of $BaO/BaTiO_3$ interfaces from first principles. Electronic structure and optical properties of $BaTiO_3$ have been calculated by Bagayoko *et al.*,[9] Saha *et al.*,[10] Cai *et al.*,[11] and more recently by Gupta *et al.*[12] Bagayoko *et al.* have studied $BaTiO_3$ in the ferroelectric (tetragonal) phase using self-consistent linear combination of atomic orbitals with a Ceperley-Alder exchange-correlation potential within the LDA. Saha *et al.* have studied both ferroelectric and paraelectric phases, approximating the ferroelectric phase with a cubic structure by using the tight binding linear muffin tin orbital method with the Barth-Hedin exchange-correlation potential. Cai *et al.* have calculated the optical properties of paraelectric (cubic) $BaTiO_3$ by using full-potential linearized augmented plane-wave (FLAPW) method within the generalized gradient approximation (GGA). Gupta *et al.* have studied $BaTiO_3$ for both cubic and tetragonal phases using FLAPW method within the LDA approximation.

Experimental studies on these compounds include infrared spectra, x-ray photoemission spectroscopy, x-ray absorption spectroscopy, and electron energy loss spectroscopy (EELS). However, we were able to find scarcely a few works on low-loss EELS studies of these compounds. Among them, Katti *et al.*[4,13] determined the local high frequency dielectric function during the cubic-to-tetragonal phase transformation in Nb doped in $BaTiO_3$ by transmission EELS.

Electron energy-loss spectroscopy is a powerful analytical technique that can be utilized to obtain information on the structure, bonding, and electronic properties of a material.[14–20] The interactions of fast electrons with the specimen result in excitations of electrons into unoccupied energy levels in the conduction band as well as collective excitations of valence electrons. When a spectrum is obtained by analyzing the energy lost by the incident electrons, the region up to an energy loss of ~50 eV is dominated by collective excitations of valence electrons (plasmon) and by interband transitions. At higher-energy losses, ionization edges occur due to excitation of core electrons into the conduction band. Interband transitions originate from the excitation of electrons in the valence band to empty states in the conduction bands, so these can be identified as transitions in a band structure model.

From the dielectric theory, it is possible to relate the experimental single scattering distribution $S(E)$, to the energy-loss function $\mathrm{Im}(-1/\varepsilon)$, by[14]

$$S(E) = \frac{I_0 t}{\pi a_0 m_0 v^2} \mathrm{Im}\left[-\frac{1}{\varepsilon(q,E)}\right] \ln[1+(\beta/\theta_E)^2], \quad (1)$$

where $\varepsilon(q,E)=\varepsilon_1+i\varepsilon_2$ is the complex dielectric function at energy loss E and momentum transfer q, a_0 the Bohr radius,

m_0 the electron rest mass, v the electron beam velocity, θ the scattering angle, $\theta_E = E/(\gamma m_0 v^2)$ is the characteristic scattering angle, γ is the relativistic factor, I_0 is the zero-loss intensity, t the specimen thickness, and β is the collection semiangle.

As peak positions in the energy-loss spectrum at low-energy losses are strongly influenced by the volume plasmon and the positions of other excitations, the energy-loss spectrum cannot be directly associated with interband transitions. However, the imaginary part of the dielectric function $\varepsilon_2(E)$ can be associated with interband transitions. The real and imaginary parts of the dielectric function can be obtained from the energy-loss function through the Kramers-Kronig analysis.[14]

It has been recognized that EELS can be used to probe changes in the electronic structure of phase transformations,[14,15,21–23] and it has been widely applied as fingerprint studies, allowing the identification of phases by comparison with well-known spectra. In the high—loss region, analysis of the first 10 eV of the spectra after the ionization edge [energy-loss near edge structure (ELNES)] can give information about the oxidation state, the absolute energy position, and about local symmetry via d level splittings in transition metal elements and orbital hybridization. The low-loss region can provide information about composition and electronic structure, as well as optical properties, although it has not found as wide application as the ELNES. The reason relies on the well-known fact that low losses originate from all possible transitions between the valence band and the conduction band. The valence band is made up of dispersed levels as opposed to almost flat core levels, and the interpretation of EELS is *a priori* more difficult.

In this work, we studied the changes in electronic structure associated with the ferroelectric transition in $BaTiO_3$ with both EELS and *ab initio* calculations with the FLAPW method, as implemented in WIEN2K code.[24,25] We found a characteristic peak at around 11 eV, appearing in the paraelectric (cubic) phase that is absent in the ferroelectric (tetragonal) phase.

The justification for this work is that, even though there has been considerable work involving both experimental and theoretical methods on $BaTiO_3$ compounds, there have been very few studies relating *ab initio* calculations with electron energy loss spectra as acquired in the electron microscope and, most of all, *in situ* studies of the phase transformation are not a common issue in the literature. In this paper, we, first of all, describe the experimental and calculation details used to reveal this characteristic peak; then, we analyze its origin by means of a careful study of the energy band structure.

II. EXPERIMENT

In this work, we used commercial $BaTiO_3$ powders (99% pure). Thin specimens suitable for electron microscopy were prepared by placing clean, dry crushed powders onto commercial folding copper grids. The ferroelectric transition temperature was found at 122 °C as determined by differential scanning calorimetry.

The ferroelectric transition was induced by placing the sample in a heating sample holder and EELS spectra were acquired at room temperature and 150 °C, corresponding to ferroelectric and paraelectric phases, respectively. In this way, we generated an *in situ* heating process that allowed us to obtain spectra for ferroelectric and paraelectric phases from the same region in the sample.

Electron energy-loss spectra were obtained using a Gatan parallel electron energy loss spectrometer (model 766) attached to a transmission electron microscope (TEM). Spectra were acquired in diffraction mode with 0.1 eV/channel dispersion, an aperture of 3 mm, and a collection semiangle of about 2.7 mrad. The resolution of the spectra was determined by measuring the full width at half maximum of the zero-loss peak and this was typically close to 1.0 eV, when the TEM was operated at 200 kV. EELS spectra were corrected for dark current and readout noise. The channel to channel gain variation was minimized by normalizing the experimental spectrum with independently obtained gain spectrum of the spectrometer. Next, all spectra were deconvoluted by the zero-loss peak recorded in a hole of the grid to obtain single scattering distributions $S(E)$.

The real and imaginary parts of the dielectric function can be obtained from the energy-loss function $\mathrm{Im}(-1/\varepsilon)$ [Eq. (1)] through the Kramers-Kronig analysis.[14] Theoretically, by measuring the absolute cross section and the thickness of the sample, we can obtain the value of the energy-loss function. However, this approach is usually not practically feasible. In order to obtain the absolute value of the energy-loss function for semiconductor materials, the refractive index at one point is needed to normalize the energy-loss spectra.[14] We have used the value of 2.4, which is an average of the ordinary and extraordinary rays, taken from the literature.[26]

III. CALCULATION DETAILS

Self-consistent band structure calculations were performed using density-functional theory (DFT) with the FLAPW method using the WIEN2K code.[24] Exchange and correlation were treated using the GGA for the potential. The core states were treated in a fully relativistic fashion. The wave functions within the muffin-tin spheres were expanded in spherical harmonics with an angular momentum of up to $l=10$. Additional local orbital extensions were used to avoid linearization errors. Nonspherical contributions to the charge density and the potential within the muffin-tin spheres were considered up to $l_{\max}=4$. In the interstitial region, plane waves with reciprocal lattice vectors up to $G=10$ were included and the plane-wave cutoff $(R_{\mathrm{MT}}K_{\max})$ was set to 7. For each compound, the muffin-tin radii were chosen as 2.5, 1.76, and 1.99 a.u. for Ba, Ti, and O, respectively. Self-consistency was considered to be achieved when the total energy variation from iteration to iteration did not exceed 10^{-5} Ry on a mesh containing 286 (288) **k** points in the irreducible Brillouin zone for the cubic (tetragonal) phase. The dielectric function can be obtained from the OPTIC Program of the WIEN2K code, Ambrosch-Draxl and Soto,[27] allowing for comparison with experiment,

$$\varepsilon_{2ii}(\omega) = \frac{4\pi^2 e^2}{m^2\omega^2 V}\sum_{v,c,k} |\langle \psi_k^v | p_i | \psi_k^c \rangle|^2 \delta(E_{\psi_k^c} - E_{\psi_k^v} - \hbar\omega). \quad (2)$$

Matrix elements are calculated from the electron states, an integration over the irreducible Brillouin zone is performed to calculate the imaginary part of the dielectric function, and then a Kramers-Kronig analysis is performed to obtain the real part of the dielectric function ε_1 and finally the energy-loss function $\mathrm{Im}(-1/\varepsilon)$. In anisotropic materials, dielectric properties must be described by the dielectric tensor which, by symmetry considerations in tetragonal structures, reduces to only two independent components $\varepsilon_{xx}=\varepsilon_{yy}$ and ε_{zz}. However, for the interpretation of EELS spectra acquired from a polycrystalline sample, the differential inelastic scattering cross section must be averaged over all angles. For samples with weak anisotropy, $\varepsilon_{zz}/\varepsilon_{xx} \approx 1$, it has been shown[28] that the dielectric function can be replaced by an "effective dielectric function" that can be written as $\varepsilon_{\mathrm{eff}} = 2/3\varepsilon_{xx} + 1/3\varepsilon_{zz}$. From our calculations, we found that the above condition is fulfilled and we have used this approximation for the effective dielectric function of the ferroelectric phase.

The crystal structure of $BaTiO_3$ in the paraelectric and ferroelectric phases has been widely studied experimentally. The paraelectric phase is cubic and belongs to the space group $Pm\text{-}3m$. The lattice constant is 4.006 Å, taken from the experimental results.[29] The unit cell contains one molecule with the Ba sitting at the origin (0,0,0), the Ti at the body center (0.5,0.5,0.5), and the three oxygen atoms at the three face centers (0.5,0.5,0), (0,0.5,0.5), and (0.5,0,0.5). The ferroelectric phase has the tetragonal structure, with space group $P4mm$ and a small tetragonal distorsion ($c/a=1.01$). The lattice parameters, taken from experimental data,[30] are $a=3.994$ and $c=4.033$ Å. The atomic positions are Ba at (0,0,0), Ti at (0.5,0.5,0.514), O_1 at (0.5,0.5,0.976), and O_2 at (0,0.5,0.485) and (0.5,0,0.485), with titanium and oxygen atoms shifted along the z direction. The shifts of the atoms in the ferroelectric phase destroy the inversion symmetry of the lattice resulting in a displacement polarization. The optical properties were calculated on a mesh containing 1140 (1183) **k** points in the irreducible part of the Brillouin zone, as many points are needed for optical calculations.

IV. RESULTS AND DISCUSSION

Figures 1(a) and 1(b) show the energy-loss function $\mathrm{Im}[-1/\varepsilon]$, from experimental (EELS) and numerical (WIEN2K) calculations, respectively, for both ferroelectric (tetragonal) and paraelectric (cubic) phases. As expected with the use of DFT methods, gaps were calculated to be smaller than experimentally observed and, in order to have a closer agreement with experiment, a scissor operation was introduced to shift the conduction band upward (1.3 eV for both phases). From Figs. 1(a) and 1(b), it is hard to find any difference between the ferroelectric and paraelectric phases that can be used to characterize one of them, besides a lack of absolute intensity when theoretical calculations are compared to experimental spectra. In F, a peak is calculated at 22.0 eV where a bump is observed experimentally and in H, a peak is calculated at 30.7 and 30.9 eV for ferroelectric and paraelectric phases, respectively, whereas in the EELS spectra, these peaks are absent. However, energy positions of the other featured points, A–E and G, coincide well between calculated and experimental ones. Calculated peaks D and G, with energies of 15.0 and 28.0 eV, come from plasmon excitations, as deduced from Fig. 2, where we have plotted the calculated real part of the dielectric function ε_1, crossing the energy axis with positive slope twice, at 14.8 and 27.7 eV. Corresponding peaks in experimental EELS in Fig. 1(a) are found at 14.4 and 27.4 eV, respectively. The other peaks A, B, C, and E come from interband transitions at 6.4, 8.8, 10.8, and 17.3 eV from numerical calculations and corresponding to 6.0, 8.4, 11.0, and 17.8 eV from experimental results.

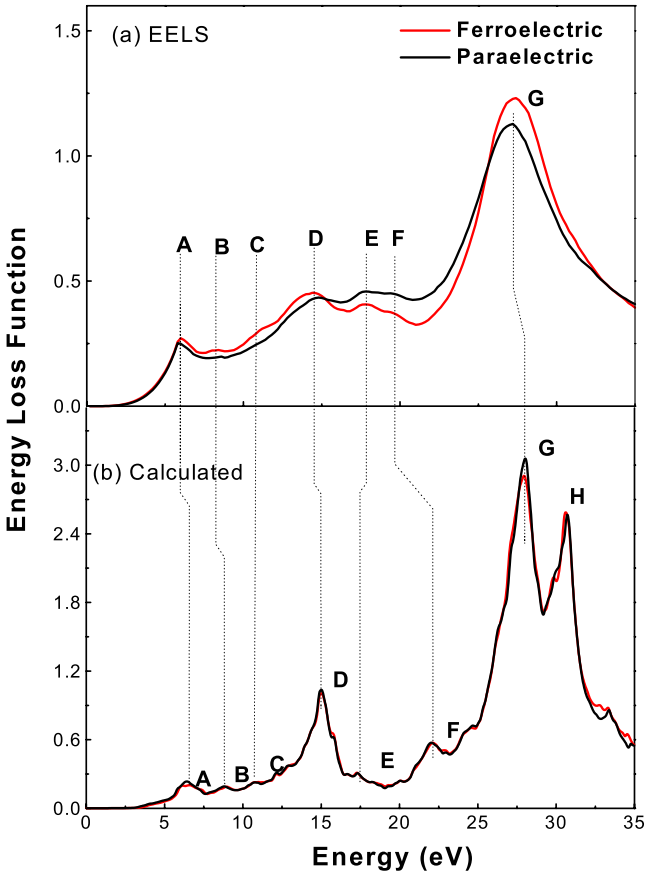

FIG. 1. (Color online) Energy-loss function $\mathrm{Im}[-1/\varepsilon]$ for ferroelectric (tetragonal) and paraelectric (cubic) phases: (a) EELS and (b) calculated.

Figures 3(a) and 3(b) show the Kramers-Kronig derived imaginary part of the experimental dielectric function ε_2 and from theoretical calculations, respectively. In the 0–10 eV, only a few small differences can be found between the ferroelectric and paraelectric phases. Main featured peaks a, b, and c in calculated spectra locate at about the same energy positions in ferroelectric and paraelectric phases at 5.5, 8.3, and 10.1 eV. However, peak d in paraelectric phase at 11.2 eV is absent in ferroelectric phase where it is observed a small plateau instead. This difference can be used to characterize the paraelectric phase, and therefore a careful analysis of the 10–15 eV region is essential to make the low-energy-loss spectroscopy an analytical tool for phase determination.

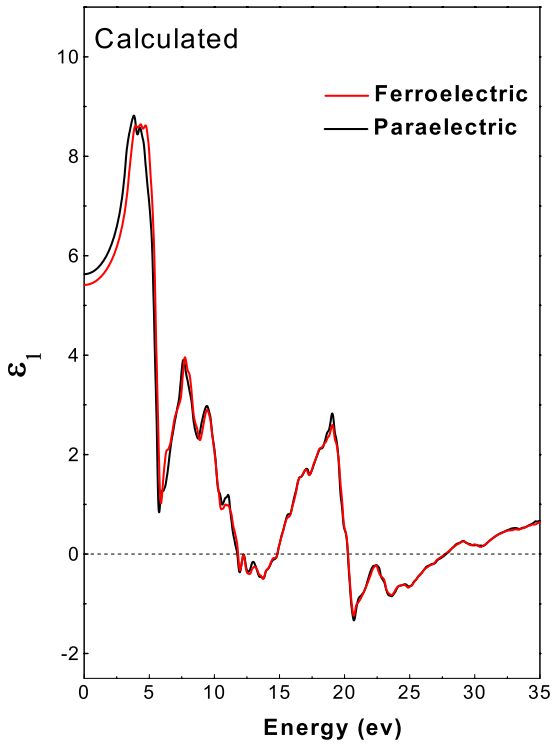

FIG. 2. (Color online) Calculated real part of the dielectric function ε_1 for ferroelectric (tetragonal) and paraelectric (cubic) phases.

Results from experimental measurements in Fig. 3(a) show good agreement with theoretical results, as long as energy peak positions is concerned, with absorptions at 5.0, 7.8, and 9.0 eV. A broad maximum extending from 11.4 and 12.0 eV in the paraelectric phase can be related with peak d in calculated spectra. The failure in observing a well-defined maximum in the experimental spectrum can be due to the deconvolution process. Here again, we observe an extended plateau at this energy for the ferroelectric phase. It should be stressed that, even though in experimental results the featured characteristics are small, they are noticeably enough to be observed in an EELS experiment with a rather limited energy resolution. We would expect the characteristic peak at ~11 eV in the paraelectric phase to be well resolved with an experiment carried out with better resolution, e.g., a field emission gun transmission electron microscope.

The most important features in these plots are the appearance of a small but clearly noticeable bump at ~11 eV in paraelectric phase which is not present in ferroelectric phase. This is not a surprising result, however, as Launay *et al.*[23] have studied titanium dioxide and reported a characteristic peak at 14 eV in low-energy-loss spectra for rutile phase that does not appear in anatase phase.

In order to get more insight into the origin of the characteristic peak at 11.2 eV, we calculated the total and partial densities of states (DOSs), as shown in Fig. 4, where the Fermi energy has been chosen at the origin on the energy axis. The total DOSs are quite similar for both phases, as can be seen from Figs. 4(a) and 4(b), and cannot provide information on the transition giving rise to the 11.2 eV peak. Here, we are looking for two regions with high DOS intensities in valence and conduction bands, whose difference is 9.9 eV (the 1.3 eV rigid band shift applied in the calculations of the optical properties has not been applied in the calculation of the density of states). As we expect this peak to originate mainly from transitions between O 2*p* to Ti 3*d* or Ba 4*d* orbitals, we have shown the angular-momentum and site-decomposed DOSs in Figs. 4(c) and 4(d). Ti 3*d* partial density of states (PDOS) presents a small but otherwise clear difference between paraelectric and ferroelectric phases, appearing a peak at 7.8 eV in paraelectric phase, which is absent in ferroelectric phase. In both cases, the O 2*p* PDOS shows maxima at energies just below −2 eV, as shown in Figs. 4(g) and 4(h). On the other hand, the Ba 4*d* PDOS is quite similar for both phases, as observed in Figs. 4(e) and 4(f), so one would be tempted to assert that the characteristic peak originates mainly with transitions from O 2*p* to Ti 3*d* orbitals. To prove this assumption, we calculated the partial imaginary part of the dielectric function, as implemented in WIEN2K, which means that we can use a smaller set of energy bands from where the construction of this partial ε_2 can be made up, arising from all possible combinations between valence and conduction bands in the chosen set. Figure 5 shows the partial ε_2 for paraelectric phase, where three sets of com-

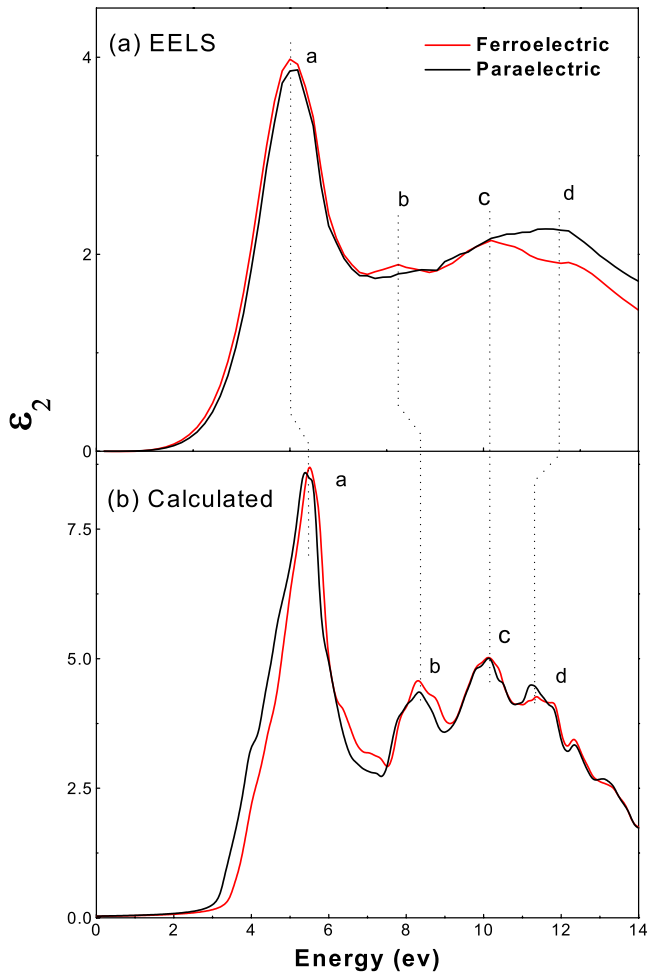

FIG. 3. (Color online) Imaginary part of the dielectric function ε_2 for ferroelectric (tetragonal) and paraelectric (cubic) phases: (a) EELS and (b) calculated.

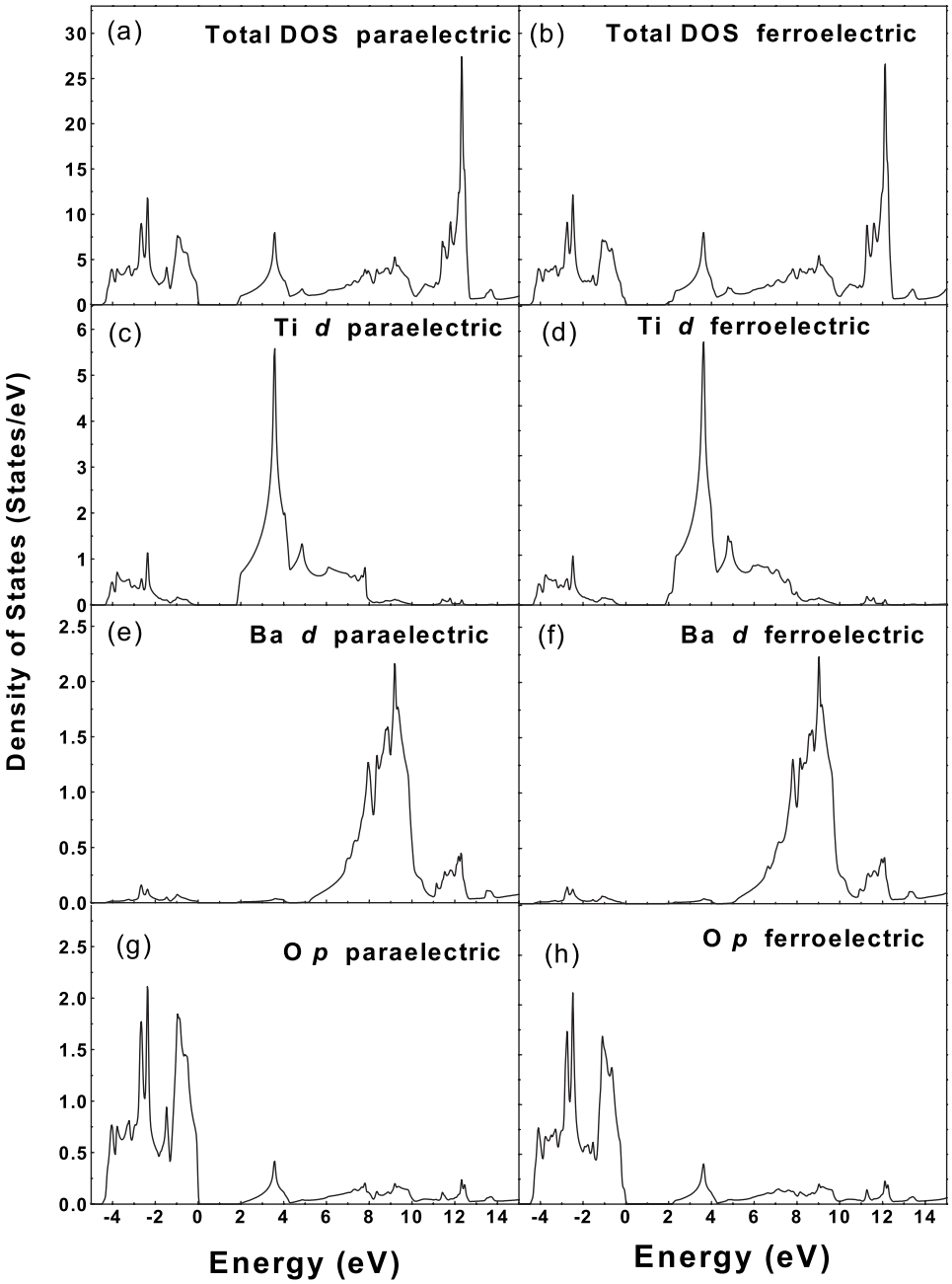

FIG. 4. Calculated total and partial density of states for ferroelectric (tetragonal) and paraelectric (cubic) phases.

binations for band to band transitions have been chosen: band 16 to band 29, band 16 to band 30, and band 17 to band 30 (highest occupied band is band number 20). Figure 5 shows that in the parelectric phase, the 11.2 eV peak comes mainly from transitions between band 16 and band 30. Identification of peaks b and c is not straightforward as they arise from combinations of many bands, as discussed above, however, peaks maxima can be attributed mainly to transitions from band 14 to band 26 for peak b (8.3 eV) and from band 19 to band 28 for peak c (10.1 eV).

Once we know the bands giving rise to the characteristic peak, these bands can be identified in an energy band plot. Referring to Eq. (2), we see that the electronic structure available in the low-loss EELS spectra is related to the occupied and unoccupied electron densities of states, the so-called joint density of states (JDOS), and to the matrix elements. The JDOS is high for energies at which two energy surfaces lie parallel to one another at a particular k point in reciprocal space. At such points, one has the so-called critical points. As single electron interband transitions depend on critical points in the band structure, peaks in the imaginary part of the dielectric function would give rise to the presence of critical points in the energy band structure.

Figures 6 and 7 show the calculated band structures for cubic and tetragonal phases, respectively. A comparison of our band structure results against those of Cai *et al.*,[11] Saha *et al.*,[10] and Kolezynski and Tkacz-Smiech[31] for the cubic structure and Bagayoko *et al.*[9] and Kolezynski and Tkacz-Smiech[31] for the tetragonal structure shows almost no discernible difference. As energy bands are extensively dis-

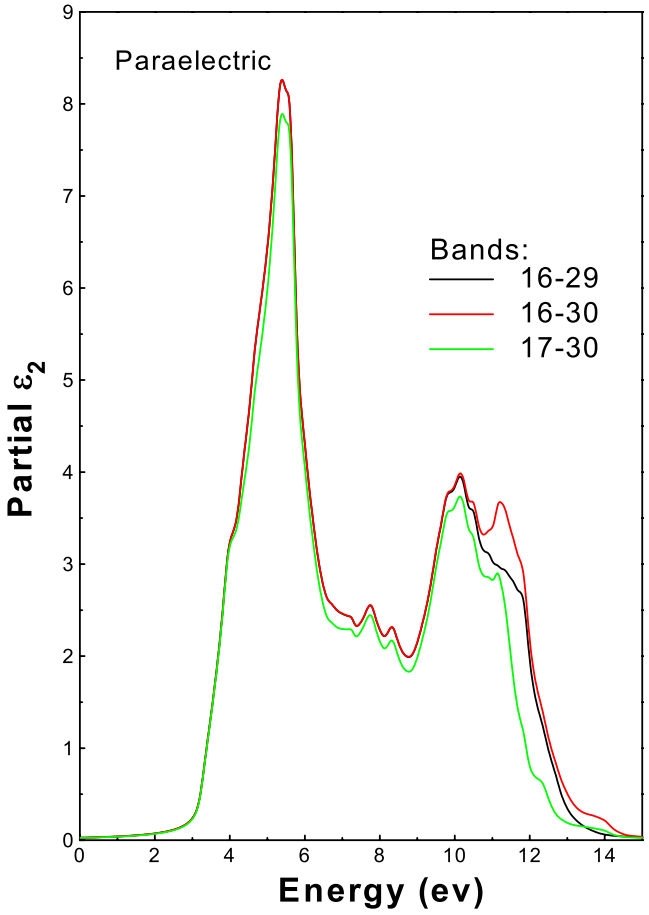

FIG. 5. (Color online) Calculated partial imaginary part of the dielectric function for paraelectric (cubic) phase. The solid line represents ε_2 when transitions from band 16 and up to band 30 have been allowed; the dotted and dashed lines represent results when band 30 or band 16 have been excluded, respectively.

cussed by these authors, we will not come to a stop in the details, except for the analysis of the characteristic peak.

In Figs. 6 and 7, the transition between band 16 and band 30 at the Γ point is indicated with an arrow and the bands are shown in thicker lines. In both cases, the energy difference is 9.9 eV, and corresponds to the energy of the characteristic peak at 11.2 eV in ε_2, originated in the transition between these bands (a 1.3 eV rigid band shift has not been applied to energy band structure calculations). Bands 16 and 30 at this point correspond mainly to O 2*p* and Ba 4*d* orbitals, respectively. Therefore, the difference between ferroelectric and paraelectric phases comes from the matrix elements, at least around 11 eV. This is particularly important because the difference characterizing the two phases lies in this energy region.

It is frequently addressed in the literature that, assuming the matrix elements are constant, peaks in the imaginary part of the dielectric function available in a low-loss EELS spectrum can be related to maxima in the density of states. However, in this case, this assumption would give rise to erroneous interpretations.

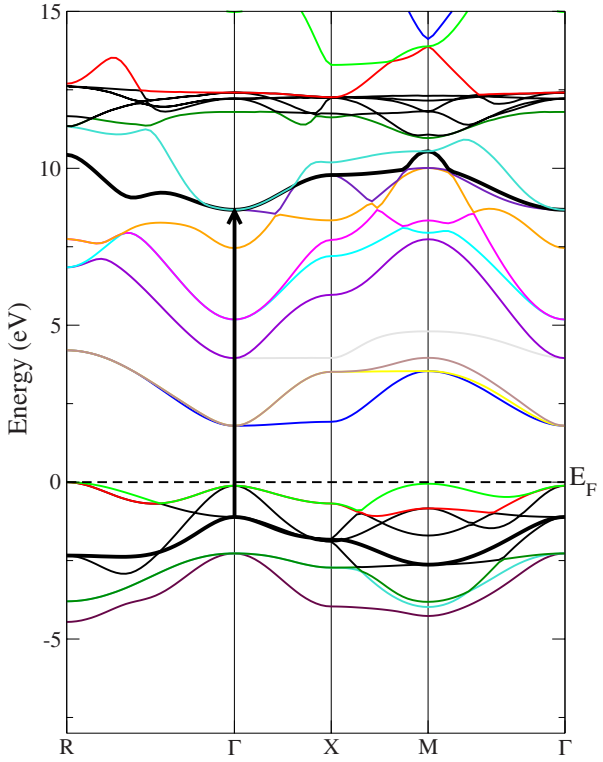

FIG. 6. (Color online) Calculated energy band structure of paraelectric (cubic) $BaTiO_3$. The arrow indicates the transition giving rise to the 11.2 eV peak in ε_2.

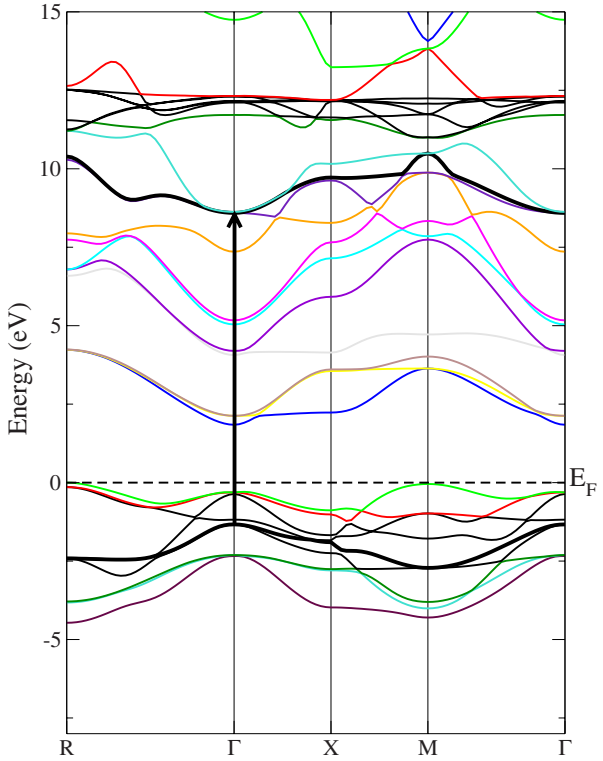

FIG. 7. (Color online) Calculated energy band structure of ferroelectric (tetragonal) $BaTiO_3$. The arrow indicates the transition giving rise to the 11.2 eV peak in ε_2.

V. CONCLUSION

The ferroelectric transition of $BaTiO_3$ has been studied *in situ* by low-loss electron energy-loss spectroscopy and spectra were acquired at room temperature and 150 °C, corresponding to ferroelectric (tetragonal) and paraelectric (cubic) phases, respectively. Results for the imaginary part of the dielectric function show a characteristic peak in the cubic structure, which provides a mean to monitor similar changes in other materials. Experimental results are compared with *ab initio* band structure calculations and good agreement was found between our experimental results and those based on theoretical calculations. The paraelectric phase characteristic peak at 11.2 eV comes mainly from transitions between O $2p$ states and Ba $4d$ states. Matrix elements in the ε_2 formulation are responsible for the difference in spectra of paraelectric and ferroelectric phases, and therefore a direct comparison with the density of states alone is not always possible. In this work, *ab initio* methods have proven to be of invaluable aid in the interpretation of EELS spectra, as it can be stated that the characteristic peak in the paraelectric phase is not an artifact in the EELS spectra.

*francisco.espinosa@cimav.edu.mx

[1] Yuan Xu Wang, Solid State Commun. **135**, 290 (2005).
[2] M. I. Kolinko, I. V. Kityk, R. Y. Bibikov, and J. Kasperczyk, J. Mater. Sci. Lett. **15**, 803 (1996).
[3] S. Piskunov, E. Heifets, R. I. Eglitis, and G. Borstel, Comput. Mater. Sci. **29**, 165 (2004).
[4] Kalpana S. Katti, Maoux Qian, Fatih Dogan, and Mehmet Sarikaya, J. Am. Ceram. Soc. **85**, 2236 (2002).
[5] R. Pirc and R. Blinc, Phys. Rev. B **70**, 134107 (2004).
[6] R. Khenata, M. Sahnoun, H. Baltache, M. Rérat, A. H. Rashek, N. Illes, and B. Bouhaf, Solid State Commun. **136**, 120 (2005).
[7] Yuan-Xu Wang, Wei-Lei Zhong, Chun-Lei Wang, Pei-Lin Zhang, and Xuan-Tao Su, Chin. Phys. **11**, 714 (2002).
[8] J. Junquera, M. Zimmer, P. Ordejón, and P. Ghosez, Phys. Rev. B **67**, 155327 (2003).
[9] D. Bagayoko, G. L. Zhao, J. D. Fan, and J. T. Wang, J. Phys.: Condens. Matter **10**, 5645 (1998).
[10] Sonali Saha, T. P. Sinha, and A. Mookerjee, Phys. Rev. B **62**, 8828 (2000).
[11] Meng-Qiu Cai, Zhen Yin, and Ming-Sheng Zhang, Appl. Phys. Lett. **83**, 2805 (2003).
[12] Garima Gupta, Tashi Nautiyal, and Sushil Auluck, Phys. Rev. B **69**, 052101 (2004).
[13] K. Katti, M. Qian, and M. Sarikaya, J. Mater. Res. **12**, 1582 (1997).
[14] R. F. Egerton, *Electron Energy Loss Spectroscopy in the Electron Miscroscope*, 2nd ed. (Plenum, New York, 1996).
[15] *Transimission Electron Energy Loss Spectroscopy in Materials Science, the Mineral, Metals and Materials Society*, edited by M. M. Disko, C. C. Ahn, and B. Fultz (Warrendale, Pennsylvania, 1992).
[16] K. Van Benthem and C. Elsässer, J. Appl. Phys. **90**, 6156 (2001).
[17] K. V. Benthem, R. H. French, W. Sigle, C. Elsässer, and M. Rühle, Ultramicroscopy **86**, 303 (2001).
[18] G. Brockt and H. Lakner, Micron **31**, 435 (2000).
[19] G. Soto, E. C. Samano, R. Machorro, M. H. Farías, and L. Cota-Araiza, Appl. Surf. Sci. **183**, 246 (2001).
[20] S. M. Bose, Phys. Lett. A **289**, 255 (2001).
[21] J. H. Hernández, M. T. Ochoa, H. Flores-Zúñiga, F. Espinosa-Magaña, and D. Ríos-Jara, J. Electron Spectrosc. Relat. Phenom. **151**, 149 (2006).
[22] D. H. Pearson, C. C. Ahn, and B. Fultz, Phys. Rev. B **50**, 12969 (1994).
[23] M. Launay, F. Boucher, and P. Moreau, Phys. Rev. B **69**, 035101 (2004).
[24] P. Blaha, K. Schwarz, G. K. H. Madsen, D. Kvasnicka, and J. Luitz, Computer code WIEN2K, Technische Universität Wien, Austria, 2001.
[25] P. Blaha, K. Schwarz, P. Sorantin, and S. B. Trickey, Comput. Phys. Commun. **59**, 399 (1990).
[26] *CRC Handbook of Chemistry and Physics*, 82nd ed., edited by D. R. Lide (CRC, Boca Raton, FL, 2001).
[27] Claudia Ambrosch-Draxl and Jorge O. Soto, Comput. Phys. Commun. **175**, 1 (2006).
[28] L. Calliari, S. Fanchenko, and M. Filippi, Carbon **45**, 1410 (2007).
[29] R. H. Buttner and E. N. Maslen, Acta Crystallogr., Sect. B: Struct. Sci. **48**, 764 (1992).
[30] J. Harada, T. Pedersen, and Z. Barnea, Acta Crystallogr., Sect. A: Cryst. Phys., Diffr., Theor. Gen. Crystallogr. **26**, 336 (1970).
[31] Andrzej Kolezynski and Katarzyna Tkacz-Smiech, Ferroelectrics **314**, 123 (2005).